Supplementary Materials for

Controlling Skyrmion Lattice Orientation with Local Magnetic Field Gradients

Duc Minh Tran,[1] Edoardo Mangini,[1] Elizabeth M. Jefremovas,[1,a)] Fabian Kammerbauer,[1] Dennis Meier,[2,3,4] Robert Frömter,[1] and Mathias Kläui*[1,3,b)]

[1]Institute of Physics, Johannes Gutenberg University Mainz, Staudingerweg 7, 55128 Mainz, Germany

[2]Department of Materials Science and Engineering, Norwegian University of Science and Technology (NTNU), Sem Sælands vei 12, 7491 Trondheim, Norway

[3]Centre for Quantum Spintronics, Norwegian University of Science and Technology (NTNU), 7491 Trondheim, Norway

[4]Faculty of Physics, University of Duisburg-Essen, Lotharstr. 1, 45057 Duisburg, Germany

Email: klaeui@uni-mainz.de

Supplementary Material 1: Image classification using U-NET

Identification of magnetic textures from MFM data was performed using a machine-learning-based pixel-wise classification approach, extended from our previous U-NET derivative convolutional neural networks (CNN)[1,2]. This model was specifically developed for the segmentation and classification of magnetic textures, such as skyrmions, in Kerr microscopy images. For classifying MFM data, the model occasionally identified poor-contrast regions and imaging artifacts as magnetic features. Therefore, an additional size-filtering step was applied to remove such regions, while ambiguous pixels attached to valid textures were retained as part of the magnetic domains.

We employ the three-class segmentation model, in which each pixel is categorized as either texture**,** background, or defect/ambiguous region (Figure S1). This classification framework enhances robustness against noise, contrast variations, and edge imperfections that commonly present in MFM images. The CNN was trained exclusively on experimental datasets containing both skyrmion and labyrinthine domain configurations to ensure good generalization across variations in image contrast and background noise. All training data were obtained from Kerr microscopy images[2]. The training employed a pixel-wise cross-entropy loss function and incorporated data augmentation (rotation, scaling, and contrast variation) to improve robustness.

Finally, for the lattice quantification, the filtered maps were post-processed to isolate skyrmions, and the skyrmion centroids were extracted. The identified skyrmion coordinates were then used to compute the local orientational order parameter $|\psi_6|$ and the global average order parameter $\langle|\psi_6|\rangle$, enabling quantitative assessment of the lattice ordering and orientation.

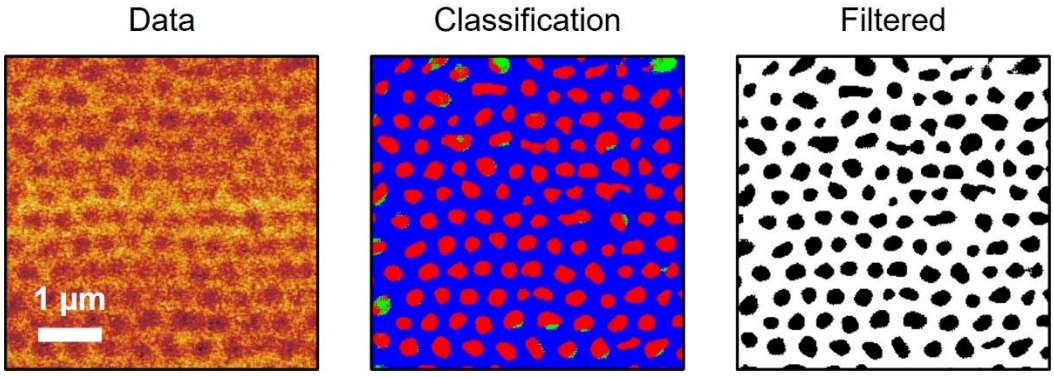

Figure S1: Classification of magnetic textures from MFM data using U-NET. Each pixel was categorized into either texture (red), background (blue), or defect (green). Artifacts that are not part of the magnetic textures were removed by applying a size filter to obtain a map of only the textures.

Supplementary Material 2: Scan line spacing Δ and domain period L correlation for efficient stripe-to-skyrmion conversion

To ensure consistency, all images in this work were processed using the same machine-learning-based classification. Skyrmions and stripes were classified based on their size and shape. The circularity is calculated as the ratio between the width and length of each texture. A value close to 1 indicates a circular shape typical of skyrmions, whereas smaller values correspond to elongated, stripe-like domains. Efficient skyrmion lattice nucleation is characterized by textures with uniform sizes and high circularity.

A clear and systematic trend is observed when Δ closely matches L: the resulting textures exhibit a narrow size distribution centered at smaller diameters, consistent with the formation of uniform skyrmions (Figure S2a). The average circularity shown in Figure S2b also increases toward unity, indicating a higher fraction of circular skyrmions. Furthermore, the total count of identified textures increases significantly as Δ approaches L, confirming efficient stripe-to-skyrmion conversion. At smaller Δ values (e.g., 62 and 125 nm), the writing scans produce a mixed state composed of residual stripes and a few isolated skyrmions, as evidenced by the broader size distribution and lower circularity values, reflecting irregularly shaped spin textures and reduced nucleation efficiency.

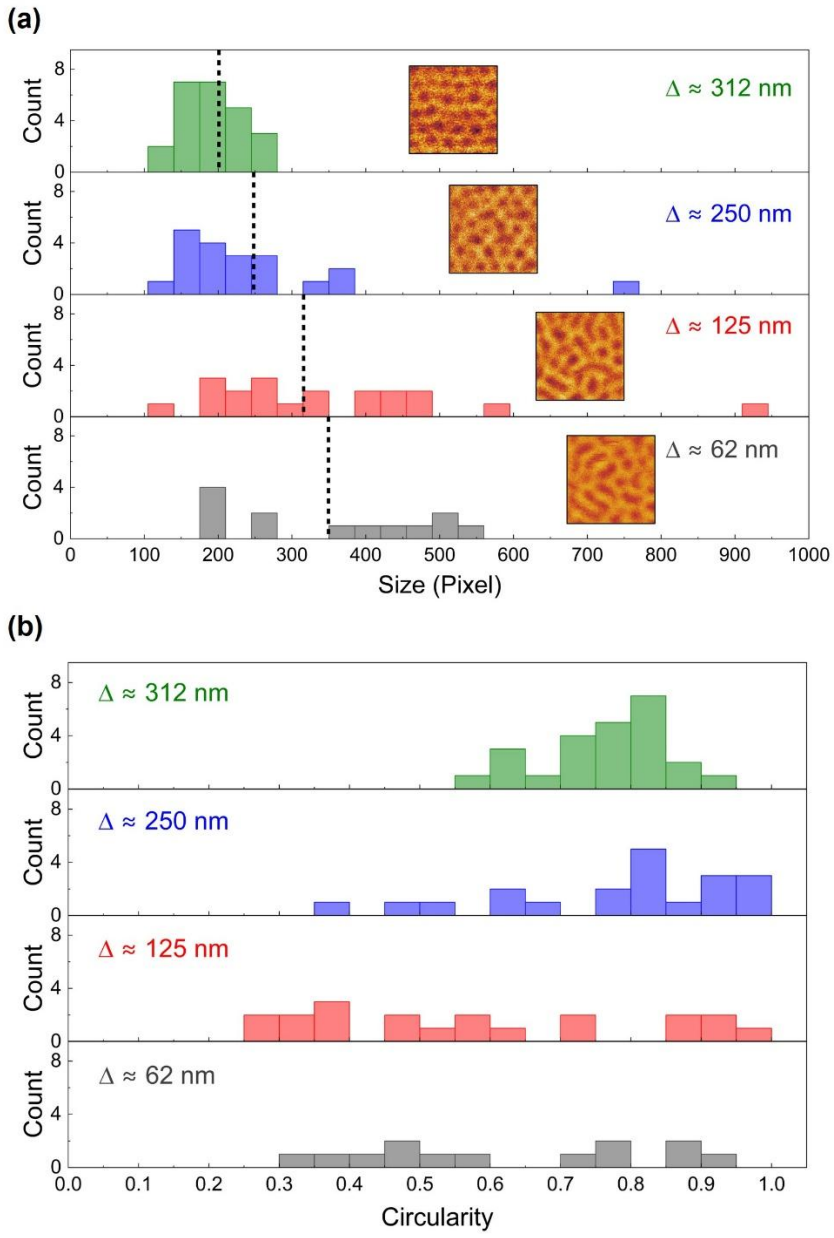

Figure S2: Statistical analysis of texture size (a) and circularity (b) after writing with single-pass MFM with different scan line spacings Δ on similar initial stripe domain periodicities of ≈ 320 nm. The dashed lines in (a) indicate the average texture size for each Δ. Insets show MFM images after writing. Scan size: 2 µm × 2 µm.

Supplementary Material 3: Ordering and orientation of spontaneously nucleated lattices

Kerr microscopy and MFM images of spontaneously nucleated skyrmions were obtained by applying a strong in-plane magnetic field pulse, a widely used approach for global skyrmion nucleation from stripe domains. In single-repetition multilayers, only short-range ordered clusters were observed with defined local orientational angles, indicated by regions of high $|\psi_6|$ values. Due to the thermally diffusive nature of skyrmions in single-layer systems, Brownian motion continuously generates topological defects that interrupt the long-range hexagonal order[3,4]. The resulting structure, shown in Figure S3a, exhibits isolated ordered domains separated by disordered boundaries (low $|\psi_6|$ values), with no global orientation angle θ.

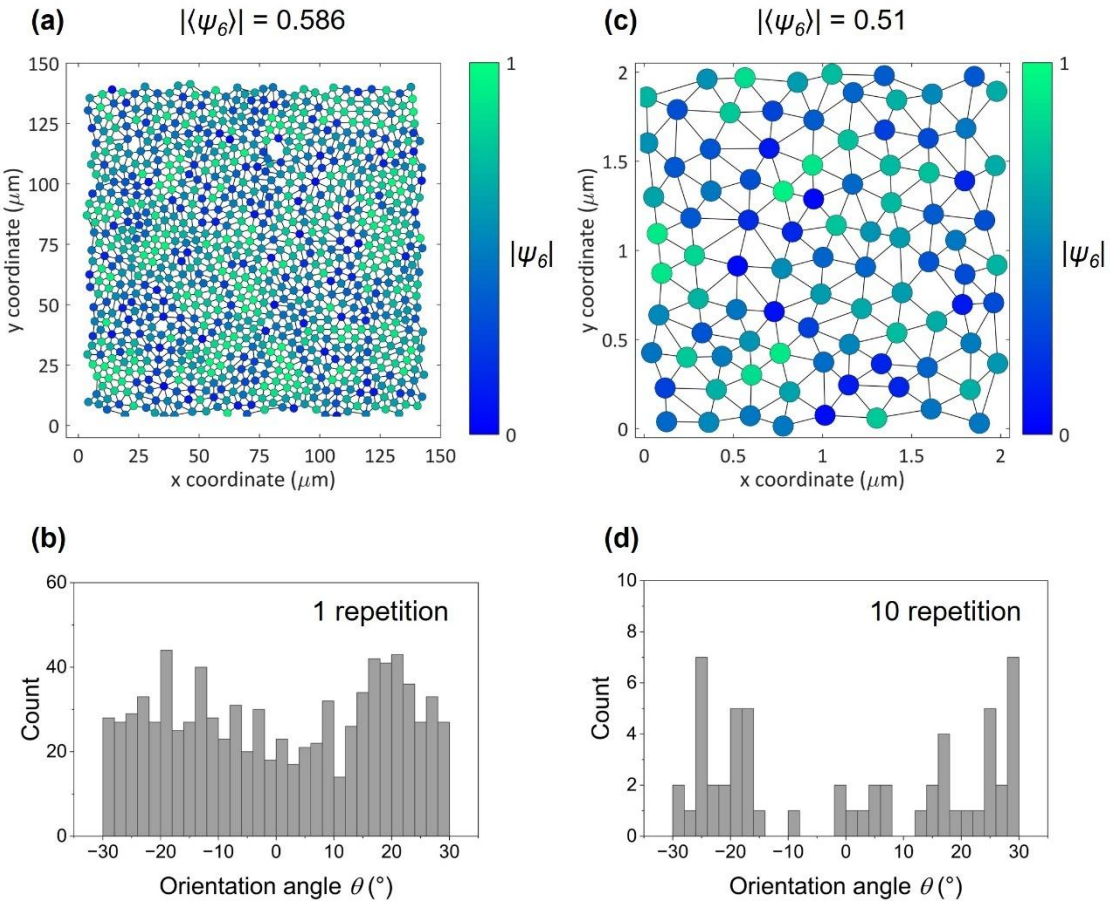

Figure S3: Mapping of $|\psi_6|$ and orientational angle analysis of spontaneously nucleated skyrmion lattices in single-repetition (a-b) and 10-repetition (c-d) stacks.

For the ten-repetition multilayer (Figures S3c-d), the interlayer exchange coupling enhances thermal stability and suppresses diffusivity, but also increases pinning, producing a largely disordered skyrmion arrangement. When scanning in “imaging mode,” the stray field is too small to induce any skyrmion rearrangements, and only local hexagonal packing without measurable lattice reorientation was consistently observed, as shown in Figure S3d.

References

1. I. Labrie-Boulay *et al.*, Phys. Rev. Appl. 21, 014014 (2024)
2. T. B. Winkler *et al.*, MOKE-microscopy-Skyrmion-dataset [Data set]. Zenodo (2024). https://doi.org/10.5281/zenodo.10997175.
3. R. Gruber *et al.*, Nat. Nanotechnol. 20, 1405–1411 (2025).
4. R. Gruber *et al.*, arXiv:2508.12988 (2025), https://doi.org/10.48550/arXiv.2508.12988.